Electronic origin of anomalously high shear modulus and intrinsic brittleness of fcc Ir

2008 J. Phys.: Condens. Matter 20 085221

(http://iopscience.iop.org/0953-8984/20/8/085221)

IOP PUBLISHING JOURNAL OF PHYSICS: CONDENSED MATTER

J. Phys.: Condens. Matter **20** (2008) 085221 (5pp) doi:10.1088/0953-8984/20/8/085221

Electronic origin of anomalously high shear modulus and intrinsic brittleness of fcc Ir

Sami Kamran[1], Kuiying Chen[2,3], Liang Chen[1] and Linruo Zhao[2]

[1] Department of Physics, University of Ottawa, Canada
[2] Institute for Aerospace Research, National Research Council Canada, Canada

E-mail: kuiying.chen@nrc-cnrc.gc.ca

Received 23 November 2007, in final form 10 January 2008
Published 7 February 2008
Online at stacks.iop.org/JPhysCM/20/085221

Abstract

Through *ab initio* density functional theory based calculations, we find that the anomalously large shear modulus and the intrinsic brittleness of face-centred cubic (fcc) iridium (Ir) are primarily a consequence of its relatively strong bonds. Comparative analysis of the bond order, which dictates the bond strength, the localization of the valence electrons and the elastic constants of Ir and a selection of fcc metals allows us to rationalize the peculiarities of Ir in terms of its strong and directional bonds. Furthermore, the similarities between the failures of Al and Ir are suggested to reflect the resemblance existing between the angular features of their bonds.

1. Introduction

In contrast to typical face-centred cubic (fcc) metals that are characterized by their ductility, iridium (Ir) has an anomalously high shear modulus and exhibits intrinsic brittleness [1]. In the past decades, a great deal of effort has been made to reveal the atomistic origins of these peculiarities in Ir. Hecker and collaborators [2, 3] were the first to speculate that the brittle cleavage in Ir is due to its intensely directional bonds. Recently, a similar explanation was set forth by Eberhart [4], who defined bond directionality in terms of the curvatures of the charge density, and correlated it with the elastic shear constant C_{44} of a series of fcc metals. Although this quantitative approach attributes very strong bond directionality to Ir, it leads to some inconsistencies when confronted with the results of the latest investigations. For instance, it gives a low value of bond directionality for Al and larger ones for Au and Cu, whilst it has been shown [5] that Al has directional bonding, and that the charge distributions of Au and Cu are rather spherically symmetric. Based on a d-band filling argument, Wills *et al* [6] associated the high shear modulus of Ir with its considerable bcc–fcc energy difference, and Gormostyrev and co-workers [7] suggested that the pseudocovalent effects, which occur as a result of the extremely directional charge redistribution of Ir under shear processing, are responsible for its high shear modulus. Nevertheless, the electronic origin of the brittle nature of Ir still remains unknown. It is noteworthy that in most previous studies, the topological features of the charge density (with or without deformation) were regarded as the major cause of the brittleness of Ir, whereas the bond strength, which is an indicator of the resistance of bonds under any change, was less exploited. In this paper, the electron localization function (ELF) and atomic bond strength of Ir, along with a selection of fcc transition metals, were calculated, and then used to elucidate the electronic origin of the abnormally high shear modulus and intrinsic brittleness of Ir.

2. Method and theory

As pointed out by De Santis and Resta [8], ELF is more suitable than the charge density to describe chemical bonds, since it amplifies the bonding features of a given electron distribution and permits us to compare the bonding of different electron distributions on an absolute scale. The explicit formula of ELF is given by

$$\mathrm{ELF} = \frac{1}{1 + \left(\frac{D(\vec{r})}{D_h(\vec{r})}\right)^2} \tag{1}$$

[3] Address for correspondence: Structures and Materials Performance Laboratory, Institute for Aerospace Research, National Research Council Canada, Montreal Road M-17, Ottawa, ON, K1A 0R6, Canada.

where

$$D(\vec{r}) = \frac{1}{2}\nabla_{\vec{r}}\nabla_{\vec{r}'}\rho(\vec{r},\vec{r}')|_{\vec{r}=\vec{r}'} - \frac{1}{8}\frac{|\nabla n(\vec{r})|^2}{n(\vec{r})} \quad (2)$$

and

$$D_h(\vec{r}) = \tfrac{3}{10}(3\pi^2)^{2/3}n(\vec{r})^{5/3} \quad (3)$$

where ρ is the first-order reduced (spin-integrated) density matrix. $D(\vec{r})$ is the von Weizsäcker kinetic energy functional, which corresponds to the ground state kinetic energy density of a non-interacting bosonic system at density $n(\vec{r})$, and $D_h(\vec{r})$ is the kinetic energy density of a uniform electron gas with a spin density equal to the local value of $n(\vec{r})$. In the case of extreme delocalization ELF assumes values close to zero, while in the case of high localization it is close to unity. In the regions where the valence charge distribution is similar to the homogeneous electron gas, the ELF comes to 0.5. For more details on ELF and its derivation, see [9].

In this study, the Vienna *Ab Initio* Simulation Package (VASP) [10, 11] was implemented to evaluate ELF using the density functional theory based projector augmented wave (PAW) method [12] with a plane wave basis set and the generalized-gradient approximation (GGA-PW91) [13]. For the ELF calculation, an fcc-based super-cell (see figure 1(a)) with periodic boundary conditions was created. The super-cell consists of eight conventional fcc unit cells, as shown in figure 1(b). The contour plots of ELF projected on the (001) plane of Au, Pt, Ir and Al are displayed in figures 2(a)–(d), respectively. The integration in the Brillouin zone of VASP calculations was performed using $8 \times 8 \times 8$ Monkhorst–Pack k-points. The plane wave cut-off energies were chosen to be ∼440 eV and the convergence of the calculations was within 10^{-5} Ryd.

Based on theoretical considerations, Bader [14] suggested that all the atomic bonding interactions fall into two categories, namely (a) the shared-electron interaction, which gives rise to covalent, dative and metallic bonds, and (b) the closed-shell interaction, which is responsible for ionic, hydrogen, electrostatic and van der Waals bonds. This classification of bonding interactions was later supported and complemented by *ab initio* calculations [15]. Consequently, the strength of metallic bonds, just like that of covalent bonds, is dictated by the predominance of the shared electrons. This information can be quantified by the bond order (BO) indices. The bond order index for atoms A and B is defined as [16]

$$B_{AB} = 2\sum_{\mu\in A}\sum_{\nu\in B}[(P^{\alpha}S)_{\mu\nu}(P^{\alpha}S)_{\nu\mu} + (P^{\beta}S)_{\mu\nu}(P^{\beta}S)_{\nu\mu}] \quad (4)$$

where P is the first-order density matrix for spins α and β, and S is the matrix of the overlap of the bases or their metric. The BO values can be calculated using the DFT based DMol3 package, which utilizes LCAO as its basis set [17]. In this work, an fcc-based cluster of 63 atoms (figure 1) was used for the BO calculations. In order to minimize the surface effects, only the bond orders between the central atom (displayed in grey in figure 1(a)) and its first nearest neighbours (FNNs) are calculated. It is worth mentioning that the values of the BO for atoms separated by distances beyond the FNN range are negligible.

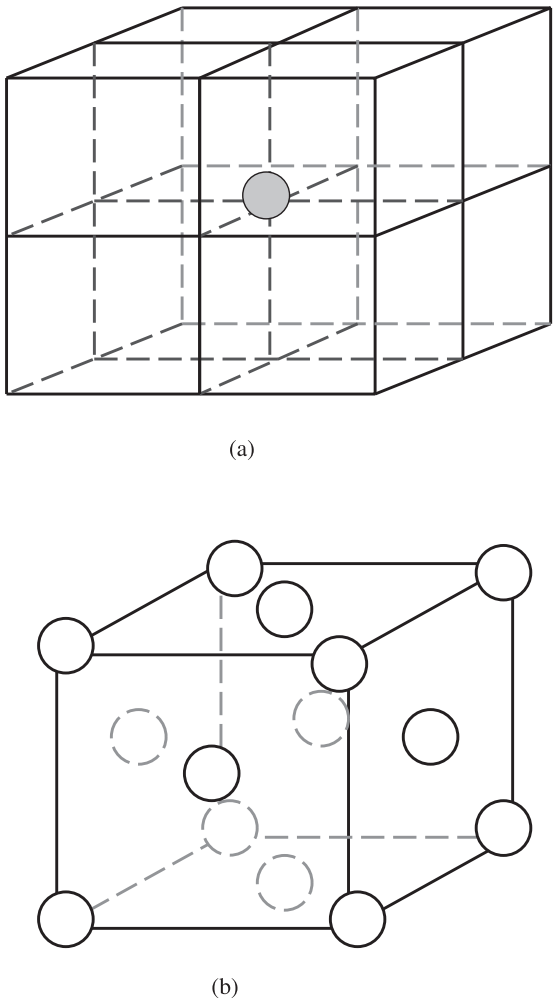

Figure 1. (a) The model used in both electron localization function (ELF) calculations (periodical boundary conditions applied along x, y and z directions) and bond order (BO) evaluations (63-atom cluster model). The model consists of eight identical fcc-based unit cells as shown in (b).

The BO, as defined by equation (4), is related to the non-classical exchange effects in the bonding. Through second quantization formalism for non-orthogonal orbitals, Mayer [18] rewrote the usual Born–Oppenheimer Hamiltonian of a diatomic molecule as a chemical Hamiltonian, which allows partitioning the energy into different terms that are chemically relevant. The chemical Hamiltonian he obtained is composed of six terms, amongst which three are proportional to BO. The full derivation of all the six terms can be found in [18]. The aforementioned terms are as follows: (i) H_2, which describes the electrostatic interactions in the point-charge approximation; in other words, it corresponds to the largest Coulomb electrostatic interactions between the ions and electrons; (ii) H_3, which corresponds to the penetration (*penetr.*) effects, i.e. the electrostatic effects arising from the deviation of the real charge distribution from the point-like distribution treated by H_2, and (iii) H_4, which accounts for the

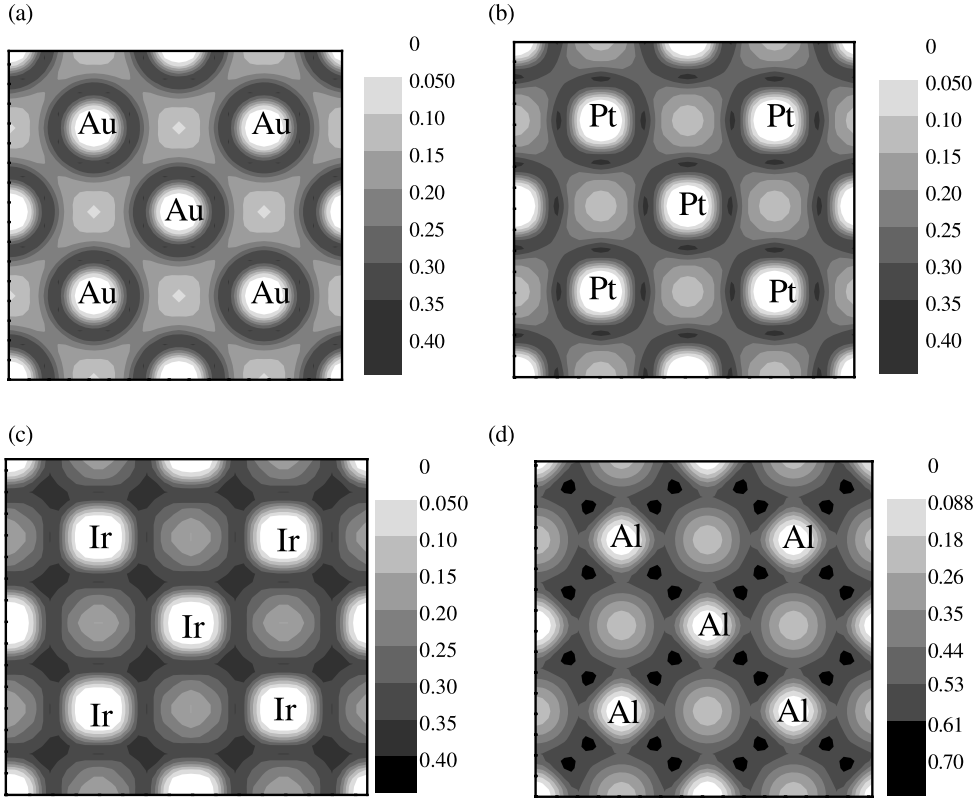

Figure 2. The ELF contour plots projected on the (001) x–y plane of (a) Au, (b) Pt, (c) Ir and (d) Al.

effects induced by the overlaps (*overl.*) between the atomic orbitals. Their proportionality relationships with BO are given by equations (5)–(9).

$$\langle \mathrm{H}_2 \rangle = \sum_{\mathrm{A<B}} (\varepsilon_{\mathrm{AB}}^{\mathrm{point}} + \varepsilon_{\mathrm{BA}}^{\mathrm{point}}) \tag{5a}$$

$$\langle \mathrm{H}_3 \rangle = \sum_{\mathrm{A<B}} (\varepsilon_{\mathrm{AB}}^{\mathrm{penetr}} + \varepsilon_{\mathrm{BA}}^{\mathrm{penetr}}) \tag{5b}$$

$$\langle \mathrm{H}_4 \rangle = \sum_{\mathrm{A<B}} (\varepsilon_{\mathrm{AB}}^{\mathrm{overl}} + \varepsilon_{\mathrm{BA}}^{\mathrm{overl}}) \tag{5c}$$

where

$$\varepsilon_{\mathrm{AB}}^{\mathrm{point}} = \frac{1}{2}\frac{1}{R_{\mathrm{AB}}}\Bigg((Z_{\mathrm{A}} - q_{\mathrm{A}})(Z_{\mathrm{B}} - q_{\mathrm{B}}) - \sum_{\lambda\in\mathrm{A}}\sum_{\omega\in\mathrm{B}} (PS)_{\omega\lambda}(PS)_{\lambda\omega}\Bigg) \tag{6}$$

$$\begin{aligned}\varepsilon_{\mathrm{AB}}^{\mathrm{penetr}} = &- \sum_{\eta,\mu,\nu\in\mathrm{A}} S^{-1}_{(\mathrm{A})\upsilon\mu}\left(\langle\chi_\mu|\left(\frac{Z_{\mathrm{B}}}{r_{\mathrm{B}}}\right)|\chi_\eta\rangle - \frac{Z_{\mathrm{B}}}{r_{\mathrm{AB}}}S_{\mu\eta}\right)\\ &\times (PS)_{\eta\nu} + \tfrac{1}{2}\sum_{\kappa,\mu,\nu\in\mathrm{A}}\sum_{\rho,\tau,\lambda\in\mathrm{B}} S^{-1}_{(\mathrm{A})\nu\mu}S^{-1}_{(\mathrm{B})\lambda\tau}\\ &\times\left([\mu\tau|\kappa\rho] - \frac{S_{\mu\kappa}S_{\tau\rho}}{R_{\mathrm{AB}}}\right)\\ &\times\left[(PS)_{\kappa\nu}(PS)_{\rho\lambda} - (PS)_{\kappa\lambda}(PS)_{\rho\nu}\right]\end{aligned} \tag{7}$$

$$\begin{aligned}\varepsilon_{\mathrm{AB}}^{\mathrm{overl}} = &- \sum_{\eta\in A}\sum_{\mu,\nu\in\mathrm{B}} S^{-1}_{(\mathrm{AB})\mu\nu}\langle\chi_\nu|\left(\frac{Z_{\mathrm{B}}}{r_{\mathrm{B}}}\right)|\chi_\eta\rangle(PS)_{\eta\mu}\\ &+ \sum_{\eta,\mu,\nu\in\mathrm{A}} S^{-1}_{(\mathrm{A})\mu\nu}\langle\chi_\nu|\left(\frac{Z_{\mathrm{B}}}{r_{\mathrm{B}}}\right)|\chi_\eta\rangle(PS)_{\eta\mu}\\ &+ \tfrac{1}{2}\sum_{\kappa\in\mathrm{A}}\sum_{\rho\in\mathrm{B}}\sum_{\lambda,\mu,\nu,\tau\in\mathrm{A}B} S^{-1}_{(\mathrm{AB})\mu\lambda}S^{-1}_{(\mathrm{AB})\nu\tau}[\lambda\tau|\kappa\rho]\\ &\times\left[(PS)_{\kappa\mu}(PS)_{\rho\nu} - (PS)_{\kappa\nu}(PS)_{\rho\mu}\right]\\ &- \tfrac{1}{2}\sum_{\kappa,\mu,\lambda\in\mathrm{A}}\sum_{\rho,\nu,\tau\in\mathrm{B}} S^{-1}_{(\mathrm{A})\mu\lambda}S^{-1}_{(\mathrm{B})\nu\tau}[\lambda\tau|\kappa\rho]\\ &\times\left[(PS)_{\kappa\mu}(PS)_{\rho\nu} - (PS)_{\kappa\nu}(PS)_{\rho\mu}\right].\end{aligned} \tag{8}$$

Here the symbol $\mu \in$ A is used to denote the assignment of spin–orbital χ_μ to atom A with Z_{A} ionic charge and q_{A} electronic charge, while R_{AB} corresponds to the distance between atoms A and B and r_{A} is the separation of electrons with respect to atom A. The short notation $[\lambda\tau|\kappa\rho]$ stands for

$$[\lambda\eta|\kappa\rho] = \int\int \chi^*_\lambda(1)\chi^*_\eta(2)\frac{1}{r_{12}}\chi_\rho(1)\chi_\kappa(2)\,\mathrm{d}\tau_1\,\mathrm{d}\tau_2 \tag{9}$$

where $\mathrm{d}\tau_i$ refers to all the variables on which the spin orbitals depend and r_{12} is the separation between spin orbitals (i.e. electrons) 1 and 2.

Moreover, BO indicates the degree to which the electrons are shared in a bond. Consequently, it quantifies the strength of shared-electron bonds, and is the theoretical equivalent of the classical bond order index, which is defined as the number of pairs of electrons shared between two atoms forming a chemical bond, i.e. the multiplicity of their bonding. Nevertheless, the values of BO are often non-integer. The deviation from integer values can be interpreted as the effects

of polarity differences between the ions or the electronic delocalization [15]. As we are studying metals, the discrepancy between the calculated values of BO and the expected value (i.e. one pair of electrons per bond) can only reflect the lack of localization.

3. Results and discussion

As can be seen from figure 2(a), the ELF contour plot of Au displays a spherical distribution, whereas the valence electrons of Pt (figure 2(b)) exhibit minor directional features, although they are relatively widely spread in the interatomic regions. This behaviour is typical of metals, since in these systems, the electrons tend to be more localized around the nuclear attractors than near the numerous valence attractors in the interstitial regions [26]. In the case of Ir, this situation is inversed: in interionic areas more electrons are localized, whereas around the ions the electron population decreases. This situation has favoured the formation of thick rod-like directional bonds in Ir, as shown in figure 2(c). However, in any of the above cases, no strong covalent bonding can be detected, since the maximal value of ELF never exceeds 0.5, even for Ir. The observed directional features of Ir are related to the d-band filling, as all transition metals with partially occupied d bands show such topological characteristics. In the case of Al (figure 2(d)), the ELF contour plot visibly shows rectangular directional bonds with sporadic high covalency (the dark spots in figure 2(d) for which ELF assumes a value of 0.7) near the ions; though the bulk of Al electrons assume a jellium-like character [8]. These bonding features of Al are due to the s–p orbital hybridization [5] and their similarity to the angular bonds of Ir accounts for the large ranges of deformation sustained by the two crystals prior to their failures [1], as directionally bonded materials usually undergo long ranges of distortion before attaining structural instability [27].

Figure 3 shows the BO values for a selection of fcc metals together with the experimental values of their shear modulus G and bulk modulus B [20]. For convenience, the order of the elements along the x-axis in figure 3 is sorted according to their atomic numbers in the periodical table. With the purpose of investigating the correlations between the BO, bond directionality and ductility of the fcc metals, the Cauchy pressure ($-(C_{12}-C_{44})$) and G/B ratio are also plotted. The Cauchy pressure provides a reliable macroscopic measure of bond directionality [21]. As for the ratio G/B, it is frequently used as an indicator of brittleness/ductility of materials [22–24]. It is evident from the plots that the BO, G and B present similar trends. All these three plots reach their peak values at Ir and have their minimum at Al. Nonetheless, the shear modulus G is better correlated with the BO. As the bond order index is proportional to the exchange component of the leading interatomic electrostatic term in the Hamiltonian of the system, it becomes clear that G is essentially related to the exchange energy, which dictates the strength of the bonds. This is further supported by the fact that aluminium, which is known for having directional bonds (see figure 2(d)), does not exhibit a peculiarly large shear modulus [5].

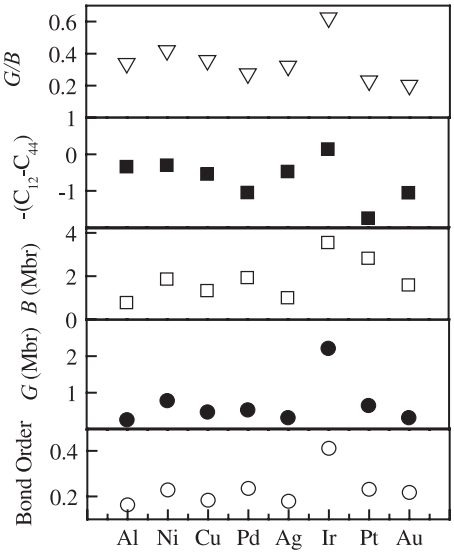

Figure 3. The calculated bond orders of selected fcc elements versus experimentally measured [20] shear (G) and bulk (B) moduli, Cauchy pressure $-(C_{12}-C_{44})$ and G/B.

The Cauchy pressure and G/B plots almost follow the same trend; however, they are only partly correlated to the BO plot. The Cauchy pressure curve agrees with our ELF contour plots as it associates high values with metals with intense directional features (like Ir, Al and Ni) and low values with those with roughly symmetric electronic distributions (like Au and Pt). The partial correlation of the G/B and Cauchy pressure with the BO indicates that the brittleness is at least partly governed by the strength and directionality of the bonds. Thus the intrinsic brittleness of Ir can be explained as follows: the relatively high exchange energy of Ir results in strong bonds that formidably resist deformation. On the other hand, once the bond is broken, its angular character renders the bond reformation hardly realizable, since the electrons have to be reorganized according to specific angles [5]. In other words, the directional character of Ir bonds reduces their mobility [25], hence promoting the brittle failure of the material.

4. Conclusions

Our calculations show that the shear modulus is principally governed by the bond strength that is proportional to the exchange energy. In the case of Ir, the contribution of the exchange energy is comparatively high, which gives rise to strong bonds capable of significant resistance against deformation, hence its anomalously large shear modulus. Furthermore, the intrinsic brittleness of Ir is shown to be a consequence of its strong bonds (i.e. high BO or exchange energy) and their intensely directional character, that considerably reduces the bond mobility of the material. These features also affect the reactivity of Ir, which is of importance in studying the properties of Ir-based alloys and needs further research.

Acknowledgments

This research is funded by the Structures and Materials Performance Laboratory of the Institute for Aerospace Research, National Research Council of Canada and also by the Natural Sciences and Engineering Research Council of Canada (NSERC).

References

[1] Panfilov P, Yermakov A, Dmitriev V and Timofeev N 1991 *Platinum Met. Rev.* **35** 126
[2] Hecker S S, Rohr D L and Stein F 1978 *Metall. Trans.* A **9a** 481
[3] Rohr D L, Murr L E and Hecker S S 1979 *Metall. Trans.* A **10a** 399
[4] Eberhart M 2001 *Phys. Rev. Lett.* **87** 205503
[5] Ogata S, Li J and Yip S 2002 *Science* **298** 807
[6] Wills J M, Eriksson O, Söderlind P and Boring A M 1992 *Phys. Rev. Lett.* **68** 2802
[7] Gornostyrev Yu N, Katsnelson M I, Medvedeva N I, Mryasov O N, Freeman A J and Trefilov A V 2000 *Phys. Rev.* B **62** 7802
[8] De Santis L and Resta R 2000 *Surf. Sci.* **450** 126
[9] Becke A D and Edgecombe K E 1990 *J. Chem. Phys.* **92** 5397
[10] Kresse G and Furthmuller J 1996 *Comput. Math. Sci.* **6** 15
[11] Kresse G and Furthmuller J 1996 *Phys. Rev.* B **54** 11169
[12] Kresse G and Joubert J 1999 *Phys. Rev.* B **59** 1758
[13] Perdew J P, Chevary J A, Vosko S H, Jackson K A, Pederson M R, Singh D J and Fiolhais C 1992 *Phys. Rev.* B **46** 6671
[14] Bader R F W 1990 *Atoms in Molecules: A Quantum Theory* (Oxford: Oxford University Press)
[15] Silvi B and Savin A 1994 *Nature* **371** 683
[16] Mayer I 1986 *Int. J. Quantum Chem.* **29** 477
[17] Delley B 1990 *J. Chem. Phys.* **92** 508
[18] Mayer I 1983 *Int. J. Quantum Chem.* **23** 341
[19] Mayer I 1983 *Chem. Phys. Lett.* **97** 270
[20] Simmons G and Wang H 1971 *Single Crystal Elastic Constants and Calculated Aggregate Properties: A Handbook* 2nd edn (Cambridge, MA: MIT Press)
[21] Johnson R A 1988 *Phys. Rev.* B **37** 3924
[22] Pettifor D G 1992 *Mater. Sci. Technol.* **8** 345
[23] Chen K, Zhao L and Tse J S 2003 *J. Appl. Phys.* **93** 2414
[24] Chen K, Zhao L and Tse J S 2004 *Phys. Lett.* A **331** 400
[25] Haydock R 1981 *J. Phys. C: Solid State Phys.* **14** 3807
[26] Silvi B and Gatti C 2000 *J. Phys. Chem.* A **104** 947
[27] Ogata S *et al* 2004 *Phys. Rev.* B **70** 104104